IEEE Access
Multidisciplinary ⋮ Rapid Review ⋮ Open Access Journal

Received 10 July 2022, accepted 10 August 2022, date of publication 16 August 2022, date of current version 25 August 2022.

Digital Object Identifier 10.1109/ACCESS.2022.3198994

RESEARCH ARTICLE

Printed Circuit Board Quality Detection Method Integrating Lightweight Network and Dual Attention Mechanism

LIGANG WU[1,2], LIANG ZHANG[3], AND QIAN ZHOU[4]
[1]College of Mechanical and Electrical Engineering, Shanxi Datong University, Datong 037003, China
[2]School of Information Science and Technology, Dalian Maritime University, Dalian 116026, China
[3]College of Coal Engineering, Shanxi Datong University, Datong 037003, China
[4]College of Business, Shanxi Datong University, Datong 037003, China

Corresponding author: Ligang Wu (ligangwu@yeah.net)

This work was supported in part by the Shanxi Provincial Philosophy and Social Science Planning Project under Grant 2021YY198, and in part by the Shanxi Datong University Scientific Research Yungang Special Project under Grant 2020YGZX014 and Grant 2021YGZX27.

ABSTRACT Printed circuit boards are versatile and highly printed, which can be widely used in various fields, and also provide new opportunities for the development of electronic information equipment. However, it is difficult to detect defects and faults during the production and use of printed circuit boards. In this paper, in view of the defects and fault detection of printed circuit boards, a deep learning detection method GSC YOLOv5 that integrates light-weight network and dual attention mechanism is proposed. First, GSC YOLOv5 is improved on the basis of YOLOv5. Ghost Conv and Ghost Bottleneck are used to realize the lightweight of the algorithm structure, reduce the number of parameters and floating point arithmetic (Flops) of the model. Second, the dual attention mechanism of Squeeze-and-Excitation Module (SE Module) and Convolutional Block Attention Module (CBAM) are introduced to optimize the performance of the algorithm, while improves the detection precision and real-time detection efficiency. Last, the experimental results show that compared with the original algorithm, GSC YOLOv5 reduces the amount of parameters and Flops by 50.38% and 55.52%, respectively, and compresses the model volume by 50.26%. Furthermore, the detection precision is increased by 2.41% and the recall rate is improved by 1.06%. At the same time, a real-times detection performance of 89.4 *FPS* is achieved, it improves by 65.18%. Therefore, the proposed algorithm is not only lightweight but also can achieve better performance, it can satisfy the detection requirements of printed circuit board.

INDEX TERMS Deep learning, lightweight, dual attention mechanism, printed circuit board, defect detection.

I. INTRODUCTION

With the development of electronic equipment and communication technology, printed circuit boards are widely used in household appliances [1], industrial equipment [2] and military facilities [3], [4]. For example, unmanned aerial vehicle, intelligent logistics and distribution vehicles, man-portable communication equipment, etc. The printed circuit board is a high-tech and strategic emerging industry encouraged by "Made in China 2025" and has a large market space and development potential.

Printed circuit boards are smaller, fully functional and have greater market advantages, but the defects detection in the manufacturing process and troubleshooting during the use of printed circuit boards are difficult and inefficient. With the development of AI detection and computer vision, solving the fault problem of circuit boards through deep learning target detection algorithms has become the current key research topic in quality inspection and troubleshooting.

At present, the commonly used deep learning algorithms include SSD [5], YOLO [6], [7], [8], [9] and Faster

The associate editor coordinating the review of this manuscript and approving it for publication was Xiaokang Yin.

R-CNN [10] etc. the combination of deep learning [11], [12] and machine vision is the development direction in the field of object detection. In the field of printed circuit board detection, Liu *et al.* [13] selected YOLOv4 as the basic framework and proposed a new loss function based on the GIOU for box regression, although recall rate of object detection and detection performance is improved, the original YOLOv4 algorithm has redundant structure and large amount of calculation. Zhang *et al.* [14] based on the standard ResNet, propose a novel cost-sensitive residual convolutional neural network model, which improved the detection accuracy and reduced the classification error.

In [15], [16], and [17], based on the two-stage target detection algorithm, a deep learning classification algorithm for circuit boards is proposed, which improves the accuracy of the classification process and promotes the construction of smart cities. In [8], the object detection model feature pyramid network is applied to PCB defect detection, which proves the effectiveness of the defect detection network. However, in [18], the environmental factors are taken into account, a deep reinforcement learning model based on the Ac-tor-Critic algorithm is proposed, and it realizes the accurate positioning and detection of the circuit board.

Deep learning algorithms are widely applied in the fault diagnosis and defect detection of circuit boards. However, the aforementioned deep learning-based detection algorithms suffer from problems such as large and complex network structures, low detection precision and slow real-time detection speed. To address these problems, this paper improves and optimizes the YOLOv5 target detection algorithm and proposes the GSC YOLOv5 that integrate lightweight network and dual attention mechanism. The main innovations and contributions of this paper are as follows:

- To achieve lightweight, Ghost Conv and Ghost Bottleneck [19] are used instead of traditional convolution and bottleneck CSP modules respectively. It not only reduces the number of model parameters and Flops, but also compresses the model volume and network layers, making the model structure simpler and lighter.
- The dual attention mechanism of SE module [20] and CBAM [21] is introduced to adjust the tendency of model feature extraction, improve model detection precision and real-time detection performance.
- Based on the integration of lightweight network and dual attention mechanism, the model structure is adjusted by ablation experiments, an algorithm model with higher detection accuracy and better real-time performance is obtained.

The remainder of this paper is organized as follows. Section II offers an printed circuit board detection system. In Section III, GSC-YOLOv5 network structure and its constituent modules are presented. Sections IV introduce the object detection performance evaluation metrics, model training parameters and processes is provided, and analyze the results of comparative experiments. Finally, conclusions and future work are given in Section V.

II. PRINTED CIRCUIT BOARD DETECTION SYSTEM

Defects in the manufacturing process of printed circuit boards affect product quality and qualification rate, and faults during use affect the service life of electronic products. It follows that the detection of the printed circuit board is crucial.

The traditional printed board detection accuracy is low and the efficiency is slow, while the detection results need to be manually marked, visualization is not obvious. In ‘‘Made in China 2025’’, the development of the printed circuit board industry is encouraged and the supporting related services are improved. Therefore, the printed circuit board production and overhaul industry came into being, which greatly promoted the development of the electronic communication industry.

In the detection and maintenance task, the printed circuit board structure is complex and not easy to find minor troubles. Therefore, the detection of printed circuit board through deep learning target detection methods has become a new development direction for circuit board detection.

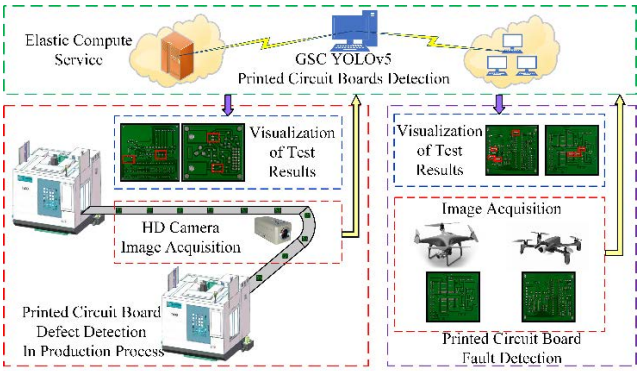

FIGURE 1. Printed circuit board detection system.

Fig.1 shows the printed circuit board detection system. Deep learning-based printed circuit board detection system can detect six types of defects, including missing hole, mouse bite, open circuit, short, spur and spurious copper. In the process of printed circuit board detection, high detection precision and wide coverage are required, while excellent data acquisition and image processing real-time performance is also desired. Therefore, deep learning-based printed circuit board detection has high requirements for the algorithm.

Based on the aforementioned practical situation and detection requirements, this paper proposes the GSC YOLOv5 algorithm, which not only compresses the model volume, reduces the consumption of hardware resources and can meet the needs of embedded development, but also improves the detection precision, recall rate and real-time detection performance, while the detection results are visualized, in line with the detection needs of printed circuit boards.

III. GSC-YOLOv5 NETWORK STRUCTURE

A. YOLOV5 ALGORITHM

The YOLOv5 target detection algorithm directly trains the model end-to-end, with excellent real-time performance and

simple network structure. It is the more flexible in the current one stage algorithm, which is extremely advantageous in the field of multi-target detection and recognition.

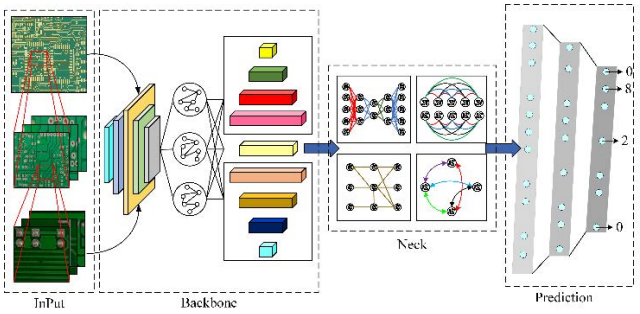

FIGURE 2. YOLOv5 algorithm process.

Fig.2 show that the four components of the YOLOv5 target detection algorithm, including input, feature extraction backbone network (Backbone), feature fusion network (Neck) and prediction. The main contents of the YOLOv5 algorithm include:

a. Input uses mosaic data enhancement to improve the detection performance of small target objects, and introduces $k-means$ clustering analysis algorithm, which adaptively completes the statistics of the detected object size.
b. The focus slicing module is used in the feature extraction backbone network to reduce the number of channels of the input images. At the same time, the introduction of cross stage partial network [22] (CSP) and spatial pyramid pooling [23] (SPP) not only effectively prevents the vanishing gradient problem caused by the deepening of the network, but also enables to obtain more fine-grained feature information.
c. In the neck structure, the feature pyramid network (FPN) module and pixel aggregation network (PAN) module are used to better fuse the features under different receptive fields, so as to output three feature maps with different scales.
d. On the output prediction stage, localization coordinates, classification information and confidence values are given by the obtained feature information, and finally completes the target recognition and positioning.

B. GHOST CONV AND GHOST BOTTLENECK

With the development of convolutional neural networks and the demand for embedded devices, deploy more efficient and lightweight neural networks with limited memory and computational resources has become the future direction of convolutional neural network development. Han *et al.* [19] fully revealed the essential features of the potential information of the feature map and proposed a more lightweight convolutional model, Ghost Conv, by applying a series of linear transformations with cheap cost using the redundancy characteristic of the feature map.

Fig.3 show the difference between traditional convolution and Ghost Conv. In the figure, Ghost Conv performs cheap linear operations $\Phi_i(i \le m)$ based on a small amount of traditional convolution, which reduces the number of parameters and Flops of the convolution process, so it has lower hardware resource requirements and GPU usage for the convolution process. Ghost Conv first generates m intrinsic feature maps based on a custom convolutional kernel size. Subsequently, the cheap linear operation is used to enhance the feature extraction of m inherent feature maps, so that each intrinsic feature map generates $s-1$ new feature maps. Finally, the m intrinsic feature maps generated by the traditional convolution and the $s-1$ new feature maps generated by the cheap linear operation are concatenated to complete the lightweight convolution operation.

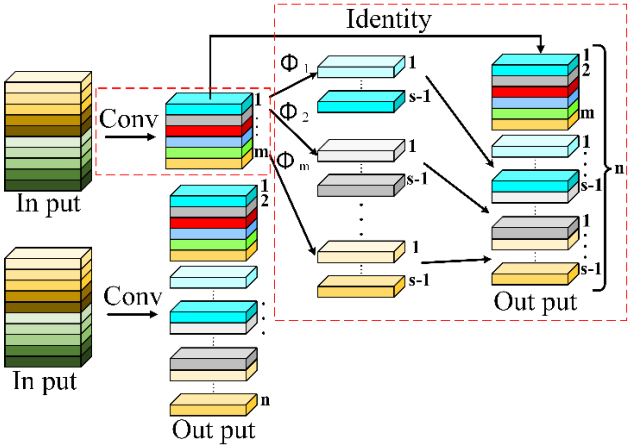

FIGURE 3. The convolution process of traditional convolution and ghost Conv.

Suppose an input image $x \in R^{c\times h\times w}$, $y \in R^{h'\times w'\times ms}$ is the output feature map with ms output channels. Thus, the amount of floating point operations required for traditional convolution can be calculated as:

$$C_T = c \times k \times k \times ms \times h' \times w' \tag{1}$$

where the number of input channels is c, $k \times k$ represents the size of custom filters in the layer. $h \times w$ and $h' \times w'$ are the height and width of the input and output image respectively.

To ensure that Ghost Conv can be used modularly, the sizes of convolution kernels, convolution stride and padding should ensure that the size of feature maps output by Ghost Conv is the same as that for a traditional convolution. Therefore, the number of computations required by Ghost Conv is

$$C_G = c \times k \times k \times m \times h' \times w' + m \times k \times k \times (s-1) \times h' \times w' \tag{2}$$

In Ghost Conv, $c \gg s$ is usually satisfied, therefore, the theoretical speed-up ratio (r_s) and model compression

ratio (r_c) of Ghost Conv and conventional convolution are as follows:

$$r_s = \frac{C_T}{C_G} = \frac{c \times k \times k \times ms \times h' \times w'}{c \times k \times k \times m \times h' \times w' + m \times k \times k \times (s-1) \times h' \times w'} \tag{3}$$

$$r_c = \frac{c \times k \times k \times ms}{c \times k \times k \times m + m \times k \times k \times (s-1)} = \frac{c \times s}{c + s - 1} \approx s \tag{4}$$

In this case, Ghost Conv can replace traditional convolution to reduce the number of parameters and compress the size of the model, and the advantages of lightweight are more obvious compared with traditional convolution. The convolutional computation of Ghost Conv is about the $1/s$ of traditional convolution, which greatly reduces the demand of hardware resources for the convolution process and drastically decreases the number of layers of the network and training time.

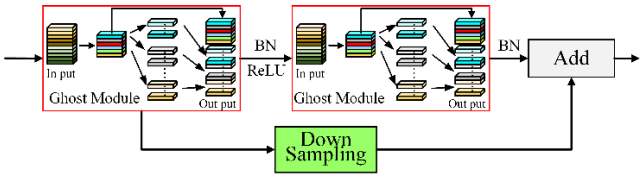

FIGURE 4. Ghost bottleneck module.

At the same time, in order to ensure the universality and convenience of the lightweight module, the lightweight module Ghost Bottleneck is shown in Fig.4, which is stacked by Ghost Conv and be taken as a plug-and-play component.

As Fig.4 shows, the Ghost Bottleneck module with *stride* = 1 consists of Ghost Conv, batch normalization (BN), down sampling and activation function. The input image is expanded by the first Ghost Conv to increase the number of channels, subsequently, reduce the number of channels by the second Ghost Conv after the BN layer and ReLU activation function to ensure that it matches the number of channels before down sampling. The Ghost Bottleneck uses fewer convolutional and BN layers compared to the CSP network, so the number of model network layers is less, and the amount of model parameters and Flops arithmetic are lower.

C. SQUEEZE-AND-EXCITATION MODULE

In convolutional operations, the desired information is obtained by extracting or fusing channel features. The introduction of the channel attention mechanism SE Module can improve the relationship between channels. In the process of feature extraction, it can adaptively adjust and correct the feature weight, increase the sensitivity of feature information and improve the saliency of the detected object.

Remarks: For any given transformation F_{tr} mapping the input X to the feature maps U where $U \in R^{H \times W \times C}$, where $H \times W$ indicates the height and width of the input image, C denotes number of channels. F_{tr} represent the transform function.

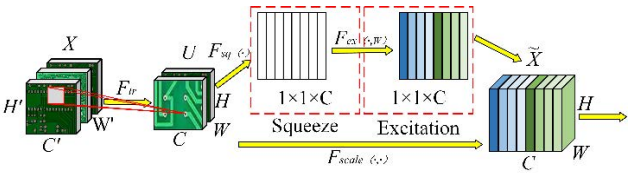

FIGURE 5. SE module schematic.

As Fig.5 shows, the SE Module goes through two steps of squeeze and excitation to access global information and recalibrate filter responses. First, the dimension of the input image is reduced by global average pooling. Second, the global information is learned through feedforward networks and the corresponding weights of each feature map are obtained. Final, the obtained corresponding weights are multiplied with the original feature map to obtain the final feature information.

In the squeeze compression stage, a feature map of $H \times W \times C$ is compressed to a size of $1 \times 1 \times C$ by global average pooling, thus a statistic z is generated by shrinking U through its spatial dimensions $H \times W$, such that the c-th element of z is calculated by:

$$z_c = F_{sq}(u_c) = \frac{1}{H \times W} \sum_{i=1}^{H} \sum_{j=1}^{W} u_c(i, j) \tag{5}$$

where z_c represents the output of compression operation, F_{sq} denotes the compression function.

Subsequently, in the excitation stage, global information obtained by squeeze compress is increase dimensioned by nonlinear activation function and full concatenation operations, therefore, the excitation operation is as follow:

$$s = F_{ex}(z, Q) = \sigma(g(z, Q)) = \sigma(Q_2 \delta(Q_1, z)) \tag{6}$$

$$Q_1 \in R^{C/r \times C}, \quad Q_2 \in R^{C \times r/C} \tag{7}$$

where δ refers to the ReLU nonlinear activation function, F_{ex} is the excitation function, z represents the output of the squeeze operation, which is also the input of the excitation operation. Q represent the mapping relationship between channels, where r is the reduction ratio of channel.

The final output of the SE module is obtained by rescaling U with the activation s:

$$\tilde{x_c} = F_{scale}(u_c, s_c) = s_c u_c \tag{8}$$

where $\tilde{X} = [\tilde{x}_1, \tilde{x}_2, \cdots, \tilde{x}_c]$ and $F_{scale}(u_c, s_c)$ refers to channel-wise multiplication between the scalar s_c and the feature map $u_c \in R^{H \times W}$ [20].

Therefore, SE module is able to accomplish adaptive adjustment of feature weights, which is more beneficial to obtain the required information.

D. CONVOLUTIONAL BLOCK ATTENTION MODULE

CBAM is a simple and efficient feed-forward convolutional attention model, which is able to sequentially infer the attention map along two separate dimensions [21], channel and spatial. Suppose given an input intermediate feature map $F \in R^{C\times H\times W}$, CBAM will complete channel feature extraction and spatial feature extraction in turn, and generate a 1D channel attention map $M_c \in R^{C\times 1\times 1}$ and a 2D spatial attention map $M_s \in R^{1\times H\times W}$, respectively. Thus the overall attention process of channel feature extraction and spatial feature extraction can be summarized as:

$$F' = M_c(F) \otimes F \tag{9}$$

$$F'' = M_s(F') \otimes F' \tag{10}$$

where $\otimes$ denotes element-wise multiplication. F'' is the final refined output.

Fig.6 shows the feature extraction process of CBAM. The average pooling can maximize the aggregation of spatial information, and the maximum pooling can obtain more refined channel features. Therefore, the CBAM module uses both average pooling and maximum pooling in the channel attention model, with the aim of improving the expressiveness of the model.

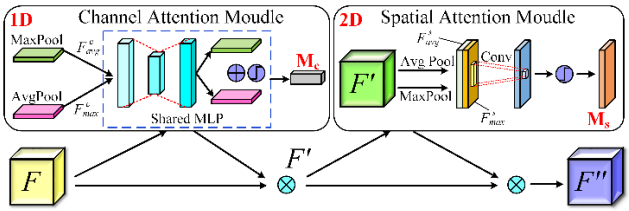

FIGURE 6. Convolutional block attention module.

In the channel attention model, first, the spatial information of the feature map is aggregated by using both average pooling and max-pooling operations. Subsequently, generating two different spatial context descriptors [21]: F^c_{avg} and $F^c_{\max}$. Last, the both descriptors will be transmitted to a shared network of multi-layer perceptron (MLP) with one hidden layer to produce a channel attention map $M_c \in R^{C\times 1\times 1}$.

The channel attention model is similar in principle to the SE Model, it uses the feature relationship between channels to generate a feature map. Since the feature information of each channel is considered and fused, the channel attention model requires a large amount of calculation. In short, the channel attention is computed as:

$$\begin{aligned} M_c(F) &= \sigma[MLP(AvgPool(F)) + MLP(MaxPool(F))] \\ &= \sigma[W_1(W_0(F^c_{avg})) + W_1(W_0(F^c_{\max}))] \end{aligned} \tag{11}$$

where, σ denotes the sigmoid function, $W_0 \in R^{C/r\times C}$ and $W_1 \in R^{C\times C/r}$, W_0 and W_1 denote the weights after pooling and sharing the network, respectively. r is the channel reduction ratio, which aims to improve the computational efficiency of the channel attention model by compressing the spatial dimensionality of the input feature map.

The spatial attention model is a complementary to the channel attention model, which can fully utilize the internal spatial relationship of feature maps to generate spatial attention maps.

In the spatial attention model, to aggregate spatial information, two 2D maps $F^s_{avg} \in R^{1\times H\times W}$ and $F^s_{\max} \in R^{1\times H\times W}$ are generated by applying max-pooling and average pooling operations, and concatenate the two 2D maps along the channel axis to generate an efficient feature descriptor. Then apply a convolution layer to generate a spatial attention map $M_s(F) \in R^{H\times W}$. In short, the spatial attention is computed as:

$$\begin{aligned} M_s(F) &= \sigma[f^{k\times k}(AvgPool(F); MaxPool(F))] \\ &= \sigma[f^{k\times k}(F^s_{avg}; F^s_{\max})] \end{aligned} \tag{12}$$

where σ denotes the sigmoid function and $f^{k\times k}$ represents a convolution operation with the filter size of $k \times k$.

Since CBAM is a lightweight and general model, it can be integrated seamlessly into any convolutional neural network structure without adding additional computational costs. Meanwhile, both CBAM and YOLO algorithms are end-to-end training models, so combining them with YOLO algorithm can complete feature extraction more efficiently and achieve more desirable results.

E. GSC YOLOV5 NETWORK STRUCTURE

Remarks: Focus is the slice module, Ghost Conv is the lightweight convolution, and Ghost Bottleneck indicate the lightweight module. SE and CBAM are the attention mechanism modules, SPP represents the spatial pyramid pooling module, which can realize the fusion of multiple receptive fields. Swish is the activation function with better performance than Leaky ReLU.

Fig.7 shows the proposed lightweight network Ghost SE CBAM YOLOv5 (GSC YOLOv5) structure. Based on the YOLOv5 algorithm, GSC YOLOv5 uses Ghost Conv and Ghost Bottleneck to replace part of the CBL and CSP module in the original algorithm, which reduces the amount of computation and Flops, making the network structure more lightweight. In addition, dual attention mechanism is introduced to enhance feature ex-traction, so that the model can obtain better detection precision and real-time detection performance.

As Fig.7 shows, the feature extraction backbone network completes feature extraction by fusing the lightweight module and the dual attention mechanism. SE and CBAM modules are used alternately after Conv and Ghost Conv, so that the feature information obtained from different convolutions can be fully utilized through weight adjustment. Al-so the alternate use of Conv and Ghost Conv is able to maintain the integrity of feature extraction as well as reduce the computation of the convolution process. In Neck, feature fusion at different scales is accomplished by convolution, C3 residual module and up sampling, which enables feature fusion to contain both underlying fine-grained and high-level semantic

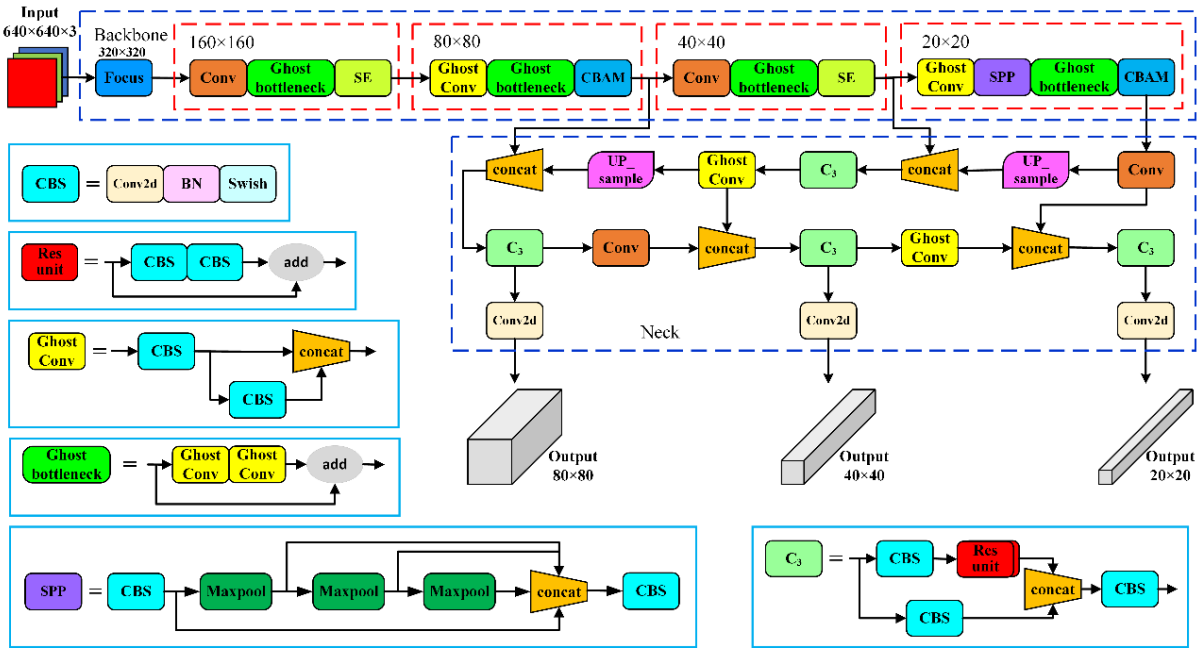

FIGURE 7. GSC YOLOv5 algorithm network structure.

information, thereby improve the detection precision and detail perception ability of the network model.

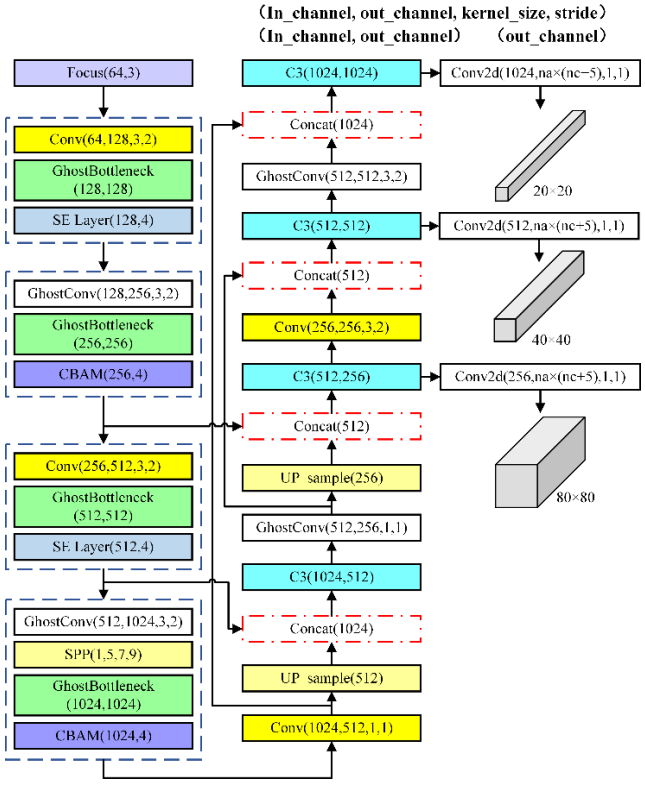

FIGURE 8. GSC YOLOv5 algorithm process and parameters.

As shown in Fig.8, after feature extraction and feature fusion, GSC YOLOv5 generates three different tensors of (256, $na\times(nc+5)$), (512, $na\times(nc+5)$) and (1024, $na\times(nc+5)$) through Conv2d at the output prediction, corresponding to three different outputs of 80 × 80, 40 × 40 and 20 × 20, respectively. Where 256, 512 and 1024 denote the number of input channels. The number of anchors for each category and the number of categories of detected objects are denoted by *na* and *nc*, respectively. The four localization parameters and one confidence parameter of anchor are represented by 5, and (1, 1) represents the size and stride of the convolution kernel.

IV. MODEL TRAINING AND RESULT ANALYSIS

A. PERFORMANCE METRICS

The Performance metrics of target detection include Accuracy index, speed index and harmonic mean index.

1) ACCURACY INDEX

Accuracy index generally precision (*P*), recall (*R*), average precision (*AP*), and other indicators (*mAP*@0.5, *mAP*@0.5 : 0.95).

Precision and recall are used to quantitatively evaluate the reliability of model during training and detection. They are calculated as follows:

$$P = \frac{TP}{TP + FP} \tag{13}$$

$$R = \frac{TP}{TP + FN} \tag{14}$$

where *TP* denotes the part of the target detection object that is correctly predicted, and *FP* is the part of the background that is mistakenly detected as the target object. The *FN* indicates the part of the target detection object that is incorrectly predicted.

The $R-P$ curve is drawn with P as the vertical coordinate and R as the horizontal coordinate, it shows the change trend of the P with the R during the training process. The AP of a category can be expressed by the size of the integral of the area under the $R-P$ curve line of that category, and the value of the integral is the AP of the category. Therefore the larger the area under the $R-P$ curve line, the higher the AP value.

The $mAP@0.5$ represents the average value of AP in N categories when the intersection over union threshold is taken as 0.5. Therefore, the $mAP@0.5$ is calculated as follows:

$$mAP@0.5 = \frac{1}{N}\sum_{i=1}^{N} AP_i(IOU_{th} = 0.5) \tag{15}$$

The $mAP@0.5:0.95$ defines the accuracy index under different values of the intersection over union threshold in N categories. It can be expressed as follows:

$$mAP@0.5:0.95 = \frac{1}{N}\sum_{i=1}^{N}\sum_{j} AP(IOU_{th} = j) \tag{16}$$

where j denotes the value taken during the change of the threshold from 0.5 to 0.95 in a stride of 0.05.

2) SPEED INDEX

The real-time detection speed of the model reflects the computing power of the algorithm, so the quality of the model is often measured by the number of real-time processing frames per second (FPS). The larger FPS, the better the real-time performance of the model.

$$FPS = \frac{n}{t} \tag{17}$$

where n denotes the number of frames of the detected picture or video in time t. Generally, the real-time detection speed is required to be greater than 30 FPS.

3) HARMONIC MEAN INDEX

The harmonic mean index F_1 comprehensively considers P and R, and is a harmonic average and trade-off between P and R. It is calculated as follows:

$$F_1 = \frac{2 \times P \times R}{P + R + \varepsilon} \tag{18}$$

where ε is a negligible minimum value, usually taken as e^{-16}.

B. MODEL TRAINING

The experiments in this paper are carried out using Python 3.8.5 environment and CUDA 11.3, under Intel Core i9-10900k@3.7GHz, NVidia GeForce RTX 3080 10G and DDR4 3600MHz dual memory hardware.

In this experiment, the dataset images of printed circuit board are 693, of which 520 are used as training set, 150 are used as validation set, and 23 are test set. Among the six fault and defect detection types, missing hole, mouse bite and spur have 115 images respectively, while open circuit, short and spurious copper consist of 116 images respectively.

In this paper, the image input is 640 × 640, the learning rate is 0.01, the cosine annealing hyper-parameter is 0.1, the weight decay coefficient is 0.0005 and the momentum parameter in gradient descent with momentum is 0.937. A total of 1000 epochs and a batch size of 12 are used during training.

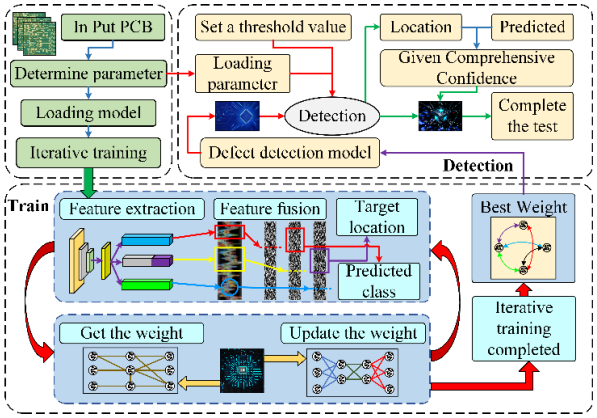

FIGURE 9. GSC-YOLOv5 algorithm printed circuit board detection process.

As shown in Fig.9, first, the pre-training preparation is completed by determining the parameters and loading the model. Second, during the training process, the required features and their optimal weights are obtained through feature extraction and feature fusion, the weight values are continuously updated through iterative training, and the loss function is gradually converged. Final, the model detection performance is continuously improved, and the trained model is used to complete the detection of printed circuit boards, so as to achieve the location and identification of printed circuit board defects and faults. Therefore, the training process of the improved and optimized GSC YOLOv5 algorithm is shown in Table 1.

C. COMPARATIVE EXPERIMENT

1) ABLATION EXPERIMENT

Ghost-SE YOLOv5, Ghost-CBAM YOLOv5 and GSC YOLOv5 are improved on YOLOv5 algorithm, other experiments are the experimental results of the above three algorithms that are not ideal in the process of network restructuring. Ghost-SE YOLOv5 and Ghost-CBAM YOLOv5 are models that introduce the SE Model attention mechanism and CBAM attention mechanism separately based on the lightweight model. GSC YOLOv5 is a model that integrates lightweight network and dual attention mechanism, which achieves the tendency of feature extraction. In addition, improves the detection accuracy and real-time detection efficiency at the same time.

Defect detection and fault diagnosis of printed circuit boards require precise identification, accurate position and excellent real-time performance of the detection process. Therefore, during the network structure adjustment and model training, the ablation experiments are shown in Table 2.

TABLE 1. Training process of GSC YOLOv5.

GSC YOLOv5 Algorithm
Determine: Parameters, Anchor, lr , L_{ciou} , IOU_{th} .
InPut: Training dataset, Training dataset, Label set.
Loading: Train models, Validate models.
Ensure: In Put, Backbone, Neck, OutPut. Algorithm environment.
N iterations of training. i -th iteration training($i \le N$):
Train Net:
a: Ghost Conv-SE, feature fusion.
b: Predicted Head: classification c_i , confidence p_i .
c: Positioning error, category error, confidence error.
d: $\sum loss$
Val Net:
a: Test effect of model ϖ_i .
b: Calculate P , R and $Val\ loss$.
c: Adjust lr and update strategy.
Save results of the i -th training: weight π_i , and model ϖ_i .
Update: **Weight:** $\pi_{i+1} \leftarrow \pi_i$, **Model:** $\varpi_{i+1} \leftarrow \varpi_i$.
Temporary storage model ϖ'
Plot: Result curve, Save best model ϖ' , Output.
End Train

During the training of the printed circuit board detection model, the total loss function is the sum of the localization loss, confidence loss, and category loss. The lower the value of the total loss function, the better the overall performance of the model, and vice versa.

The total loss function convergence curves of GSC YOLOv5, YOLOv5, Ghost-SE YOLOv5 and Ghost-CBAM YOLOv5 are shown in Fig.10.

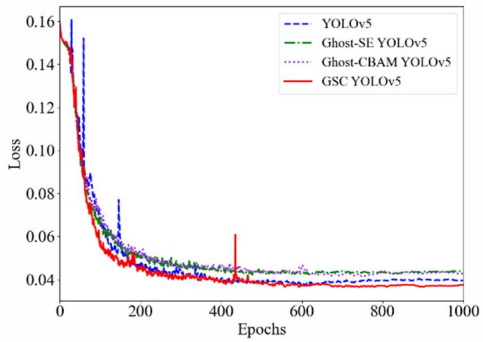

FIGURE 10. Loss function convergence curves.

As shown in Fig.10, compared with the original YOLOv5 algorithm, GSC YOLOv5 has a lower loss function convergence value during the model training process, so it has higher detection precision and localization accuracy, as well as better confidence and classification performance.

2) PRECISION AND RECALL

During the training process, the P and R improve continuously with the increase of iteration times and eventually converge. The P and R curves of the printed circuit board detection model are shown in Fig.11 (a) and Fig.11 (b), respectively.

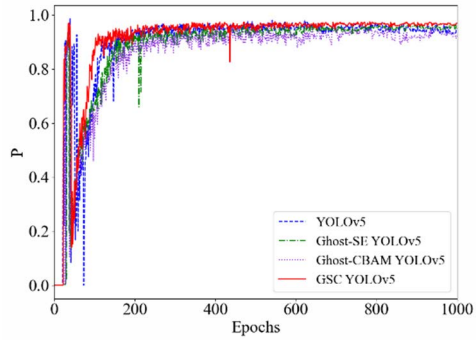

(a) Precision convergence curve

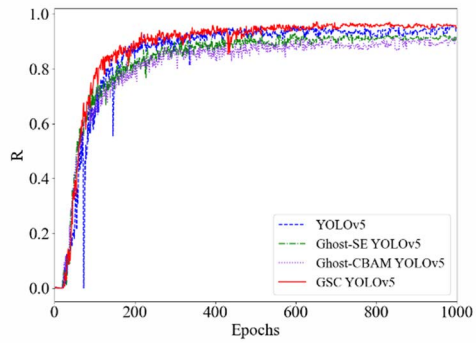

(b) Recall convergence curve

FIGURE 11. Precision and Recall convergence curve.

GSC YOLOv5 in the printed circuit board detection process, detection precision and recall rate of 97.0% and 95.0%, respectively, which are improved by 2.41% and 1.06% respectively compared with the original YOLOv5 algorithm.

During the training of the printed circuit board detection model, the $mAP@0.5$ and $mAP@0.5:0.95$ accuracy curves are shown in Fig. 12(a) and 12(b), respectively. It can be observed that the accuracy curve of GSC YOLOv5 algorithm is more ideal than other algorithms, not only the accuracy of the model increases faster in the early training stage, but also the final convergence value is higher than other algorithms. Based on the original YOLOv5 algorithm, the GSC YOLOv5 algorithm $mAP@0.5$ is improved by 0.87% and $mAP@0.5:0.95$ is improved by 1.54%.

The $R-P$ curve is an important performance indicator of measure the reliability of a model. During the training process of the model, the P and R show a negative correlation, indicating the variation of the P with the R. The larger the area under the $R-P$ curve, the higher the P of the model.

Fig.13 shows the $R-P$ curves of different models during the training process. As shown in the figure, the area under the $R-P$ curve of the GSC YOLOv5 algorithm is significantly larger than that of YOLOv5, Ghost-SE YOLOv5 and Ghost-CBAM YOLOv5, so $AP_{GSCYOLOv5} > AP_{YOLOv5}$.

In summary, in the printed circuit board defect and fault detection model training process, GSC YOLOv5 algorithm

TABLE 2. Result of ablation experiment.

Model	P	R	mAP@0.5	mAP@0.5:0.95	Model Volume/M	GPU utilization	Flops/G	Network Layer
YOLOv5	0.945	0.939	0.956	0.492	95.3	7.34	116	499
Ghost-SE YOLOv5	**0.949**	0.917	0.935	0.463	**34.8**	**3.72**	**34.0**	**306**
Ghost-CBAM YOLOv5	0.926	0.904	0.933	0.459	**34.8**	**3.88**	**34.6**	**326**
GSC YOLOv5 (Our)	**0.970**	**0.950**	**0.965**	**0.507**	**47.4**	**5.45**	**51.6**	**301**
Other Experiments	0.923	0.901	0.925	0.462	**34.4**	**3.59**	**33.8**	**285**
	0.917	0.888	0.911	0.445	**33.6**	**4.33**	**33.0**	**289**
	0.931	0.898	0.926	0.457	**34.4**	**4.34**	**33.8**	**289**
	0.938	0.897	0.927	0.460	**34.4**	**3.56**	**33.8**	**288**
	0.924	0.891	0.916	0.451	**33.6**	**3.55**	**33.0**	**288**
	0.925	0.898	0.923	0.458	**33.9**	**4.31**	**33.1**	**307**
	0.930	0.898	0.921	0.457	**34.8**	**4.32**	**34.0**	**307**
	0.902	0.888	0.908	0.448	**33.9**	**3.79**	**33.1**	**306**
	0.927	0.902	0.930	0.457	**34.0**	**3.84**	**33.7**	**326**
	0.953	**0.945**	0.955	0.491	**47.4**	**5.44**	**51.6**	**301**
	0.955	**0.959**	**0.967**	**0.506**	**47.6**	**5.45**	**51.6**	**301**
	0.964	**0.951**	**0.961**	**0.500**	**47.4**	**5.45**	**51.6**	**301**

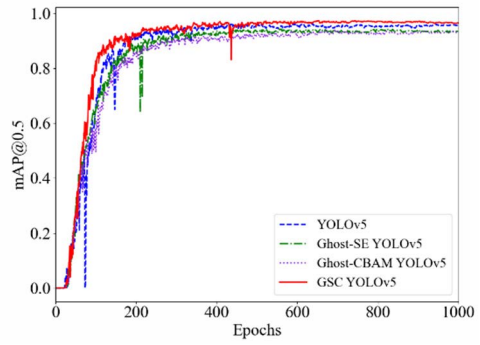

(a) $mAP@0.5$ **accuracy curve**

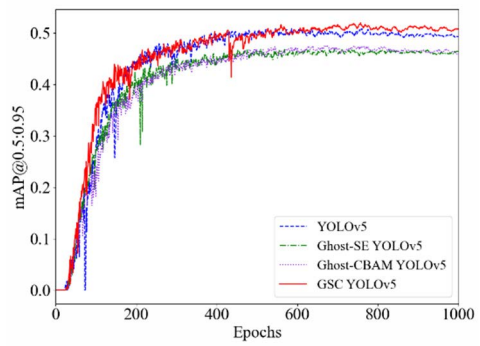

(b) $mAP@0.5:0.95$ **accuracy curve**

FIGURE 12. ***mAP*@0.5 and *mAP*@0.5 : 0.95 convergence curve.**

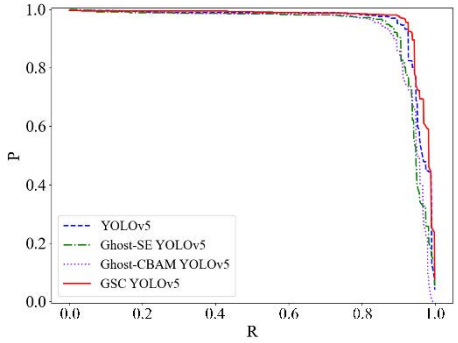

FIGURE 13. ***R* – *P* curves of different algorithm.**

loss function convergence faster, and all accuracy indexes are higher than the original YOLO algorithm, so, the proposed algorithm can meet the practical requirements in the process of printed circuit board detection.

3) HARMONIC MEAN PERFORMANCE

The harmonic mean performance F_1 comprehensively considers P and R, and is represented by the harmonic mean curve, it shows the change trend of the comprehensive performance of the model at different confidence ($conf$).

The detection of defects and faults of printed circuit boards has equally high requirements for the detection accuracy and recall, the higher the accuracy, the more precise for localization and identification, and the higher the recall, the wider for the detection coverage. Therefore, balancing accuracy and recall in the detection process is an important prerequisite and guarantee to verify the reliability of the proposed algorithm.

The harmonic mean curve of different algorithm is shown in Figure 14, it can be observed that the original YOLOv5 algorithm obtains the maximum value of $F_1 = 0.94$ at $conf = 0.252$, while the GSC YOLOv5 algorithm achieves

the maximum value of $F_1 = 0.96$ at $conf = 0.515$, which is improved by 2.0% compared to the original algorithm.

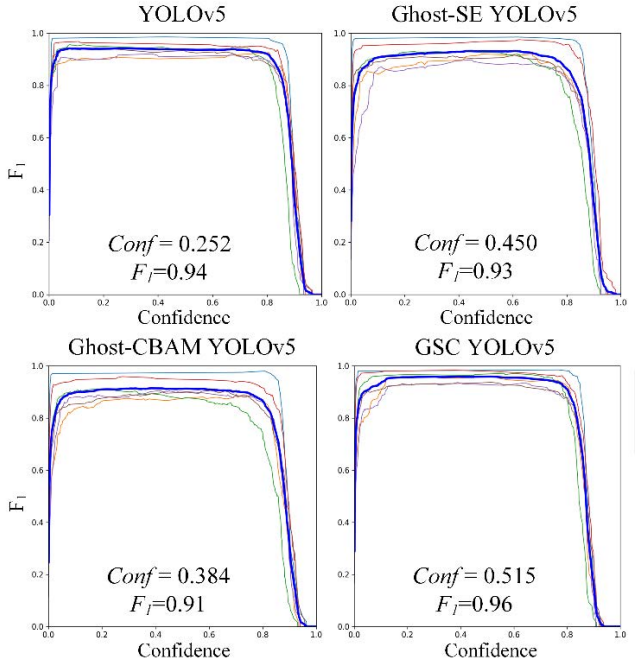

FIGURE 14. Harmonic mean curve.

It can be seen that in the process of trade-off between P and R, the GSC YOLOv5 algorithm can show a stronger harmonic advantage, while the confidence level of 0.5 is also more scientific, so the proposed algorithm can show better performance in the printed circuit board detection process.

4) RESULT ANALYSIS

Fig.15 shows the training process parameters comparison between GSC YOLOv5 and the original YOLOv5 algorithm. As the figure shows, the improved GSC YOLOv5 algorithm reduces the number of parameters from 47.42 million to 23.53 million, which is a decrease of about 50.38%. Furthermore, the Flops, model volume, network layers and GPU occupancy are reduced by 55.52%, 50.26%, 39.68% and 25.75%, respectively.

It is obvious that in the case of introducing Ghost Conv and Ghost Bottleneck, the proposed algorithm model achieves lightweight.

Fig.16 shows the comparison of experimental results in terms of P, R and F_1. As the figure shows, the P of GSC YOLOv5 is increased from 0.945 to 0.970, which is 2.5% higher than that of YOLOv5 algorithm. At the same time, the R and F_1 are improved by 1.1% and 2.0%, respectively.

The experimental results show that the introduction of the dual attention mechanism improves the propensity of feature extraction, increases the saliency of the detected objects, and improves the model detection performance.

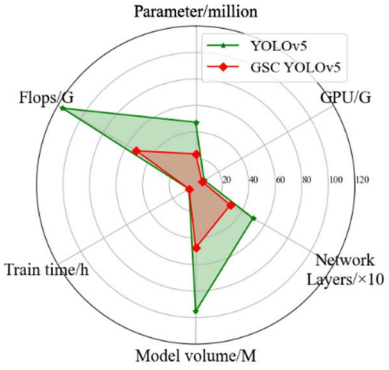

FIGURE 15. Parameters comparison of training process.

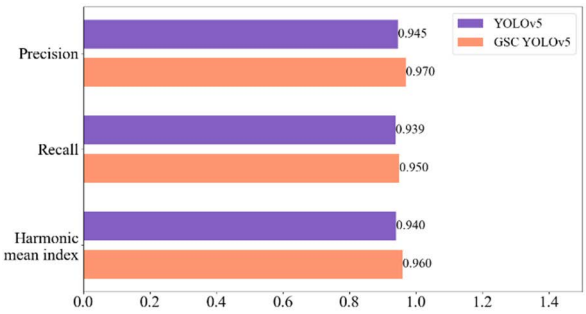

FIGURE 16. Comparison of experimental results.

In deep learning target detection, real-time detection performance is required to be greater than 30 *FPS*. Printed circuit board defects and faults detection of the original YOLOv5 algorithm real-time detection speed of 54.12 *FPS*, but the improved GSC YOLOv5 algorithm real-time detection speed of up to 89.40 *FPS*, compared to the original algorithm to improve 65.18%. Therefore, GSC YOLOv5 algorithm can meet the requirements of real-time detection.

In summary, the GSC YOLOv5 algorithm not only reduces the number of model parameters and network layers, but also compresses the model size and GPU occupancy, achieving a lightweight effect. At the same time, the detection accuracy, recall rate and re-al-time detection performance all show advantages over the original algorithm, so the effectiveness of the proposed algorithm is verified through experiments.

The printed circuit boards in different scenarios were selected for testing and validation, and a detection results of different algorithms is shown in Fig.17. The experimental results show that the GSC YOLOv5 target detection algorithm is more accurate in the application of practical scenarios, and the confidence level of detection and classification is higher. In the defect and fault detection of the same circuit board, the missing detection rate is lower and the comprehensive detection effect is better of GSC YOLOv5.

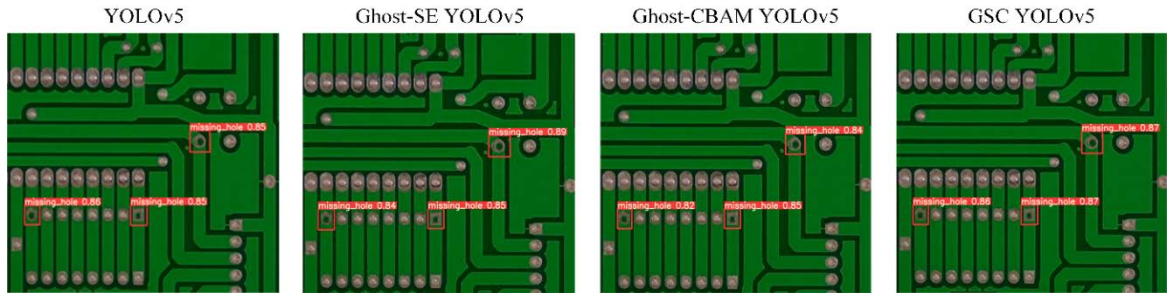

(a) Missing hole

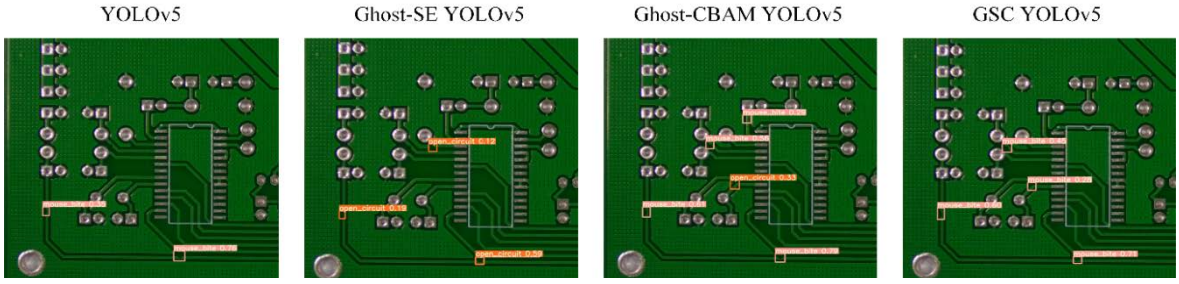

(b) Mouse bite

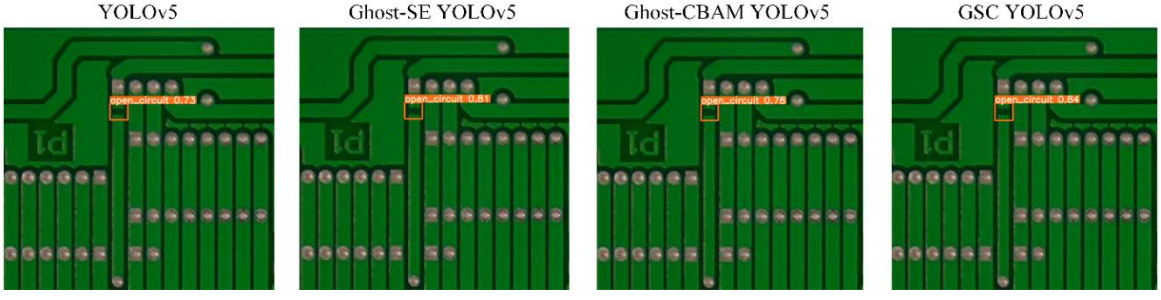

(c) Open circuit

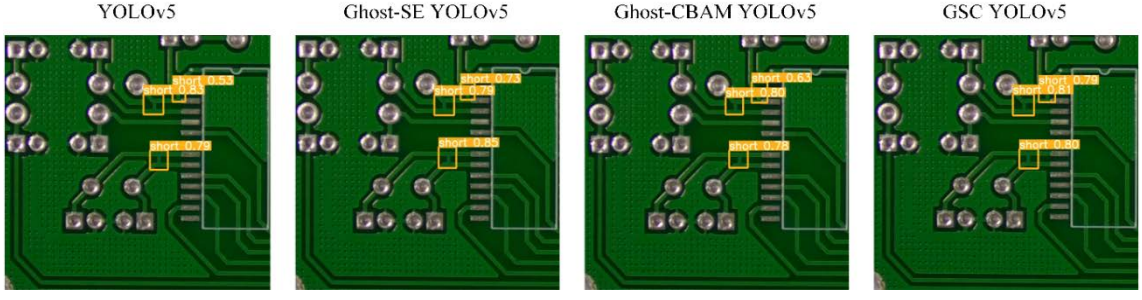

(d) Short

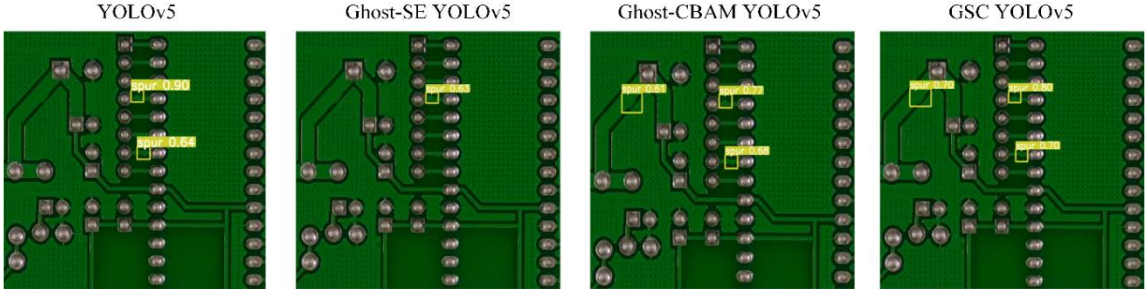

(e) Spur

FIGURE 17. Comparison of test results.

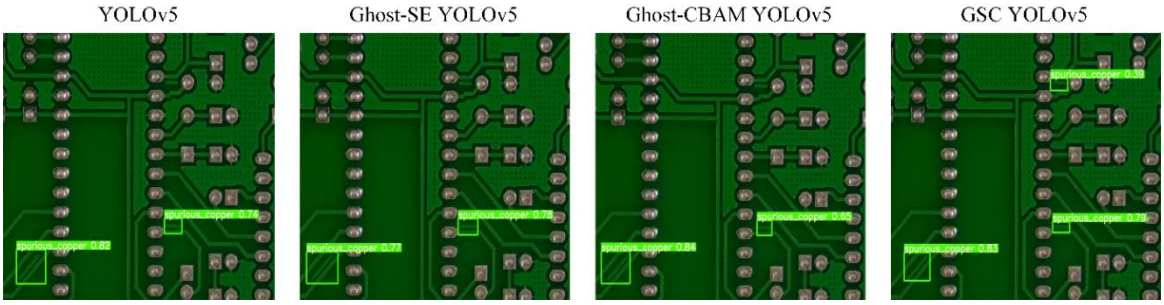

(f) Spurious copper

FIGURE 17. *(Continued.)* **Comparison of test results.**

From the test results in Fig.17 (a), it can be seen that the detection results of missing hole in the same printed circuit board are the same, and all the defects can be detected, but the improved GSC YOLOv5 algorithm detects the results with higher confidence compared to the original algorithm.

From the test results in Fig.17 (b), it can be seen that the original YOLOv5 algorithm has the case of missed detection, while the introduction of a single attention mechanism has the case of false detection. Compared to the GSC YOLOv5 algorithm, which has higher detection precision and is able to detect all the fault points.

From the test results in Fig.17 (c) and (d), it can be seen that the improved GSC YOLOv5 algorithm detects the results with higher confidence compared to the original algorithm.

From the test results in Fig.17 (e), it can be seen that the YOLOv5 algorithm misses a fault detection point. After introducing the attention mechanism, the detection result of CBAM is better than that of SE, which is due to the fact that CBAM has one more spatially directed feature extraction mechanism than SE, and therefore the detection results are more accurate. However, among the above detection results, the GSC YOLOv5 algorithm has higher detection accuracy, fault coverage and confidence level.

From the test results in Fig.17 (f), it can be seen that the improved GSC YOLOv5 algorithm has a higher coverage of detection and can detect more fault points.

V. CONCLUSION

In this paper, the GSC YOLOv5 lightweight neural network algorithm was proposed, which reduces the hardware requirements and achieves better detection effect by integrating lightweight network and dual attention mechanism. In the process of printed circuit board detection, more comprehensive defects can be detected and higher detection confidence can be given. Therefore, the GSC YOLOv5 meets the demand for high precision and high efficiency detection of printed circuit boards. On this basis, the effective combination of deep learning and reinforcement learning algorithm to achieve a more ideal effect is the next research direction.

REFERENCES

[1] Q. Liu, C. Feng, Z. Song, J. Louis, and J. Zhou, "Deep learning model comparison for vision-based classification of full/empty-load trucks in earthmoving operations," *Appl. Sci.*, vol. 9, no. 22, p. 4871, Nov. 2019, doi: 10.3390/app9224871.

[2] M. Pal, P. Palevičius, M. Landauskas, U. Orinaitė, I. Timofejeva, and M. Ragulskis, "An overview of challenges associated with automatic detection of concrete cracks in the presence of shadows," *Appl. Sci.*, vol. 11, no. 23, p. 11396, Dec. 2021, doi: 10.3390/app112311396.

[3] L. Cai, L. J. Yu, J. X. Yan, Z. W. Li, P. Ren, X. Bai, E. Yang, and Y. G. Liu, "Autonomous detection of damage to multiple steel surfaces from 360° panoramas using deep neural networks," *Comput.-Aided Civil Infrastruct. Eng.*, vol. 36, no. 12, pp. 1585–1599, 2021.

[4] Y. He, K. Song, Q. Meng, and Y. Yan, "An end-to-end steel surface defect detection approach via fusing multiple hierarchical features," *IEEE Trans. Instrum. Meas.*, vol. 69, no. 4, pp. 1493–1504, Apr. 2020.

[5] W. Liu, D. Anguelov, D. Erhan, C. Szegedy, S. Reed, and C. Fu, "SSD: Single shot multibox detector," in *Computer Vision—ECCV* (Lecture Notes in Computer Science). 2016, pp. 21–37, doi: 10.1007/978-3-319-46448-0_2.

[6] J. Redmon, S. Divvala, R. Girshick, and A. Farhadi, "You only look once: Unified, real-time object detection," in *Proc. IEEE Conf. Comput. Vis. Pattern Recognit. (CVPR)*, Jun. 2016, pp. 779–788, doi: 10.1109/CVPR.2016.91.

[7] J. Redmon and A. Farhadi, "YOLO9000: Better, faster, stronger," in *Proc. IEEE Conf. Comput. Vis. Pattern Recognit. (CVPR)*, Jul. 2017, pp. 6517–6525, doi: 10.1109/CVPR.2017.690.

[8] Q. Zhang and H. Liu, "Multi-scale defect detection of printed circuit board based on feature pyramid network," in *Proc. IEEE Int. Conf. Artif. Intell. Comput. Appl. (ICAICA)*, Jun. 2021, pp. 911–914, doi: 10.1109/ICAICA52286.2021.9498174.

[9] Q. F. Zhang and H. R. Liu, "Classification of the trap-neuter-return surgery images of stray animals using YOLO-based deep learning printed with a majority voting system," *Appl. Sci.*, vol. 11, no. 8, p. 8578, 2021, doi: 10.3390/app11188578.

[10] B. Hu and J. Wang, "Detection of PCB surface defects with improved faster-RCNN and feature pyramid network," *IEEE Access*, vol. 8, pp. 108335–108345, 2020, doi: 10.1109/ACCESS.2020.3001349.

[11] X. Wu, Y. Ge, Q. Zhang, and D. Zhang, "PCB defect detection using deep learning methods," in *Proc. IEEE 24th Int. Conf. Comput. Supported Cooperat. Work Design (CSCWD)*, May 2021, pp. 873–876, doi: 10.1109/CSCWD49262.2021.9437846.

[12] V. A. Adibhatla, J.-S. Shieh, M. F. Abbod, H.-C. Chih, C.-C. Hsu, and J. Cheng, "Detecting defects in PCB using deep learning via convolution neural networks," in *Proc. 13th Int. Microsyst., Packag., Assem. Circuits Technol. Conf. (IMPACT)*, Oct. 2018, pp. 202–205, doi: 10.1109/IMPACT.2018.8625828.

[13] X. Liu, J. Hu, H. Wang, Z. Zhang, X. Lu, C. Sheng, S. Song, and J. Nie, "Gaussian-IoU loss: Better learning for bounding box regression on PCB component detection," *Expert Syst. Appl.*, vol. 190, Mar. 2022, Art. no. 116178, doi: 10.1016/j.eswa.2021.116178.

[14] H. Zhang, L. Jiang, and C. Li, "CS-ResNet: Cost-sensitive residual convolutional neural network for PCB cosmetic defect detection," *Expert Syst. Appl.*, vol. 185, Dec. 2021, Art. no. 115673, doi: 10.1016/j.eswa.2021.115673.
[15] I. A. Soomro, A. Ahmad, and R. H. Raza, "Printed circuit board identification using deep convolutional neural networks to facilitate recycling," *Resour., Conservation Recycling*, vol. 177, Feb. 2022, Art. no. 105963, doi: 10.1016/j.resconrec.2021.105963.
[16] J. Lian, L. Wang, T. Liu, X. Ding, and Z. Yu, "Automatic visual inspection for printed circuit board via novel mask R-CNN in smart city applications," *Sustain. Energy Technol. Assessments*, vol. 44, Apr. 2021, Art. no. 101032, doi: 10.1016/j.seta.2021.101032.
[17] Y. Lu, B. Yang, Y. Gao, and Z. Xu, "An automatic sorting system for electronic components detached from waste printed circuit boards," *Waste Manage.*, vol. 137, pp. 1–8, Jan. 2022, doi: 10.1016/j.wasman.2021.10.016.
[18] C. Solorzano and D.-M. Tsai, "Environment-adaptable printed-circuit board positioning using deep reinforcement learning," *IEEE Trans. Compon., Packag., Manuf. Technol.*, vol. 12, no. 2, pp. 382–390, Feb. 2022, doi: 10.1109/TCPMT.2022.3142033.
[19] K. Han, Y. Wang, Q. Tian, J. Guo, C. Xu, and C. Xu, "GhostNet: More features from cheap operations," in *Proc. IEEE/CVF Conf. Comput. Vis. Pattern Recognit. (CVPR)*, Jun. 2020, pp. 1577–1586, doi: 10.1109/CVPR42600.2020.00165.
[20] J. Hu, L. Shen, S. Albanie, G. Sun, and E. Wu, "Squeeze-and-excitation networks," *IEEE Trans. Pattern Anal. Mach. Intell.*, vol. 42, no. 8, pp. 2011–2023, Aug. 2020, doi: 10.1109/TPAMI.2019.2913372.
[21] S. Woo, J. Park, J. Y. Lee, and D. Korea, "CBAM: Convolutional block attention module," in *Proc. 15th Eur. Conf.* Munich, Germany: Springer, 2018, pp. 3–19, doi: 10.1007/978-3-030-0123402_1.
[22] C.-Y. Wang, H.-Y. M. Liao, Y.-H. Wu, P.-Y. Chen, J.-W. Hsieh, and I.-H. Yeh, "CSPNet: A new backbone that can enhance learning capability of CNN," in *Proc. IEEE/CVF Conf. Comput. Vis. Pattern Recognit. Workshops (CVPRW)*, Jun. 2020, pp. 1571–1580, doi: 10.1109/CVPRW50498.2020.00203.
[23] K. He, X. Zhang, S. Ren, and J. Sun, "Spatial pyramid pooling in deep convolutional networks for visual recognition," *IEEE Trans. Pattern Anal. Mach. Intell.*, vol. 37, no. 9, pp. 346–361, Jan. 2015, doi: 10.1007/978-3-319-10578.

LIGANG WU was born in Datong, Shanxi, China, in 1986. He received the M.Sc. and Ph.D. degrees in control theory and control engineering from Dalian Maritime University, Dalian, China, in 2012 and 2016, respectively. He is currently an Associate Professor with the College of Mechanical and Electrical Engineering, Shanxi Datong University. His current research interests include machine learning algorithms, intelligent control, intelligent manufacturing, and other artificial intelligence fields.

LIANG ZHANG was born in Lvliang, Shanxi, China, in 1995. He received the B.E. degree in automation specialty from Shanxi Datong University, Datong, China, in 2019, where he is currently pursuing the graduate degree in source and environment. His research interests include machine learning algorithms, object detection, recognition, and localization.

QIAN ZHOU was born in Nanchong, Sichuan, China, in 1988. She received the M.Sc. degree in business management from the Southwestern University of Finance and Economics, Chengdu, China, in 2014. Her current research interest includes data processing.